Proceedings of the 7th World Congress on Momentum, Heat and Mass Transfer (MHMT'22)
~~Lisbon, Portugal~~ Virtual Conference – April 07 – 09, 2022
Paper No. ENFHT 222
DOI: 10.11159/enfht22.222

The Effect of Locations of Inlet and Outlet Manifolds on Thermal Performance of a Lithium-Ion Battery Thermal Management System

Kuuku-Dadzie Botchway, Mohammad Reza Shaeri
Department of Mechanical Engineering, University of the District of Columbia, Washington, DC 20008 USA
kuuku.botchway@udc.edu; mohammadreza.shaeri@udc.edu

Abstract **-** The dependency of thermal performance of a liquid-cooled battery thermal management system (TMS) on the locations of inlet and outlet manifolds was investigated. Seven battery cells with a volumetric heat generation were located in an in-line configuration inside the TMS. In the front-inlet (FI) TMS, the water entered and exited alongside the cells while in the side-inlet (SI) design, the water entered and exited from the lateral side of the TMS. The simulations were performed at two flow rates of 0.5 and 1.0 LPM. Both TMSs maintained the temperature variations below 4.1 °C within the cells at two flow rates. While almost the same maximum temperature was obtained for a given cell using FI and SI designs at the higher flow rate, the SI design resulted in a lower maximum temperature at the lower flow rate. Also, the SI TMS at 0.5 LPM resulted in slightly higher maximum temperatures for given cells compared with the FI design at 1.0 LPM. However, since the pumping power is proportional with the flow rate, the SI design is a promising TMS with a potential of minimizing the pumping power despite a slight penalty in the thermal performance compared to the FI design.

Keywords**:** Thermal management; Liquid-cooled system; Lithium-ion battery; Pumping power; CFD.

1. Introduction

Lithium-ion batteries (LIBs) are the key components of electric vehicles (EVs) and have been identified as suitable energy storage systems in EVs due to their high energy, high specific power, and long cycle life [1]. The performance of a LIB is directly impacted by its temperature such that low and high battery temperature leads to a decrease in the battery capacity, and thermal runaway, respectively [2]. The optimal range of working temperature for LIBs is between 25-50 °C, with a temperature gradient below 5 °C [3]. As a result, to provide safer and reliable operational conditions for LIBs and, successful commercialization of EVs, thermal issues in LIBs must be addressed by effective thermal management systems (TMSs) [4]. Liquid-cooled systems have been identified as effective TMSs due to their excellent cooling performances and reliability [5]. However, existences of design limitations such as space, weight, etc., restrict implementing specific ranges of sizes, dimensions, and configurations of a TMS's features like the locations of inlet and/or outlet manifolds. These restrictions become more serious when the TMS is used for a LIB pack with specific layouts to fit in allowed space and dimension. This study presents a practical insight to the thermal performances of two different LIB's TMSs with different locations for the inlet and outlet manifolds at different flow rates.

2. Problem Description and Computational Procedure

Fig. 1 illustrates the schematic of TMSs in this study. Seven cells, Cell 1 to 7 in Fig. 1(a), as representative of the battery cells, with a diameter and height of 18 mm and 65 mm, respectively, are located in an in-line configuration inside the TMS. The cell number increases by increasing the distance from the inlet. The cell properties are selected based on the properties provided in [6], as specific heat, thermal conductivity, and density equal to 1027 $J.kg^{-1}.K^{-1}$, 25 $W.m^{-1}.K^{-1}$, and 4035 $kg.m^{-3}$, respectively. From two side of each cell, a height of 17.5 mm is exposed to the outside, and the rest of cell (i.e., 30 mm) is covered by the TMS. Two different TMS designs are considered in this study, which their differences are in the locations of inlet and outlet manifolds. In the front-inlet (FI) design, the water (i.e., coolant) enters and exits the TMS alongside the cells while in the side-inlet (SI) design, the water enters and exists from the lateral side of the TMS. Both inlet and outlet diameters are 12 mm in both TMSs. For the simplicity, the case of each TMS has zero thickness. By assumption of a laminar, steady, and incompressible flow, the constant properties for both the fluid and solid, and a constant heat generation inside the cells, the governing equations to simulate the flow and heat transfer are as follows:

Continuity: $$\nabla . \boldsymbol{u} = 0 \quad (1)$$
Momentum conservation: $$(\boldsymbol{u}.\nabla)\rho\boldsymbol{u} = -\nabla p + \mu\nabla^2\boldsymbol{u} \quad (2)$$
Energy conservation (fluid): $$\boldsymbol{u}.\nabla T_f = \frac{\lambda}{\rho c_p}\nabla^2 T_f \quad (3)$$
Energy conservation (solid): $$k\nabla^2 T_s + \dot{q} = 0 \quad (4)$$

where ρ, u, p, μ, λ, c_p, and T_f are the fluid density, velocity, pressure, viscosity, thermal conductivity, specific heat, and temperature, respectively, and k and T_s are the solid thermal conductivity and temperature, respectively. Also, $\dot{q}$ is the volumetric heat generation in the battery cell. In this study, a constant value of $\dot{q} = 300\,\mathrm{KW.m^{-3}}$ is assumed for individual cell, which represents the critical condition at large discharge rates of LIBs [7]. To calculate the temperature distribution on the interface of the solid and fluid, the conjugate problem of heat conduction equation with convection in the fluid are solved, simultaneously [8]. The simulations are performed at two volume flow rates of 0.5 and 1.0 LPM (liter/min). A grid structure with 354,000 elements was selected after performing grid independence tests and reaching negligible changes in the magnitudes of heat transfer coefficients and friction coefficients by increasing the number of elements beyond 354,000. For the inlet boundary conditions, a flow rate and a temperature of 22 °C are set for the water at the inlet. The outlet boundary conditions are set by imposing zero axial gradients for all the variables at the outlet. To set the outlet boundary conditions correctly, the outlet is located far enough from the surface of the TMS. The remaining faces are walls with a no-slip boundary condition. A convection heat transfer with the convective heat transfer coefficient of 1 $\mathrm{W.m^{-2}.K^{-1}}$ and an ambient temperature of 27 °C, respectively, is considered for all the surfaces of cells and TMS that are exposed to the air. The transport equations are solved using ANSYS FLUENT.

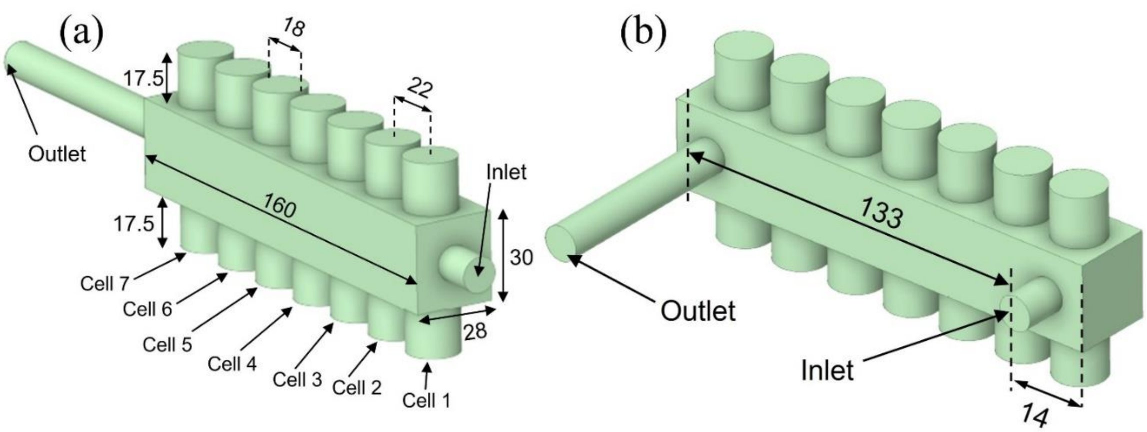

Fig. 1: Three-dimensional view of: (a) FI TMS; (b) SI TMS. Unit is in mm.

3. Results

The maximum Reynolds number (based on the inlet diameter) is ~1765, which represents a laminar flow throughout the simulations. Fig. 2 illustrates the temperature variation within an individual cell, which corresponds to the difference between the maximum and minimum temperature of the cell. Both TMSs maintained temperature variations between 3.5 °C and 4.1 °C within all cells at both flow rate. At both flow rates the maximum temperature variation among all cells in each TMS is less than 0.5 °C; as a result, both TMSs maintain the temperature variation within an individual cell and among different cells in the TMS below an acceptable limit for safe operations of LIBs.

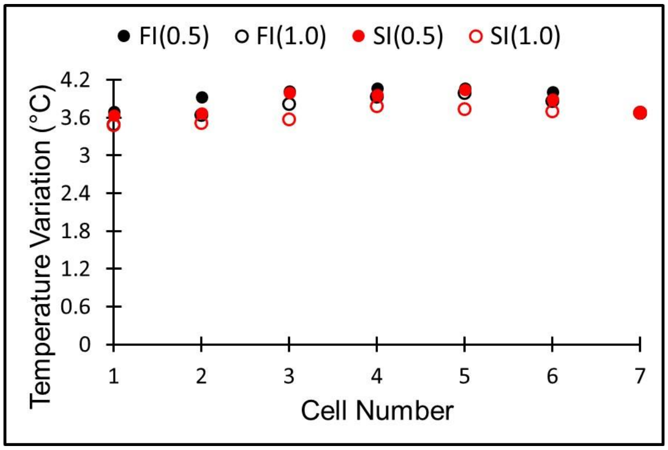

Fig. 2: Temperature variation within individual cells. The number inside the parenthesis stands for the flow rate in LPM.

Fig. 3 illustrates the maximum temperature of an individual cell at different flow rates. For a given TMS, an increase in the flow rate corresponds to an increased sensible heat, which results in reduction in the cell temperature. A monotonic increase in the cell temperatures by increasing the distance from the inlet is due to an increase in the coolant's temperature along the TMS. However, one exception is the last cell (i.e., Cell 7), which experiences lower temperature than its adjacent cell, because the last cell is surrounded only by Cell 6 and exchanges heat only by this cell. As a result, the peak of temperature reaches at Cell 6, and after that the temperature decreases.

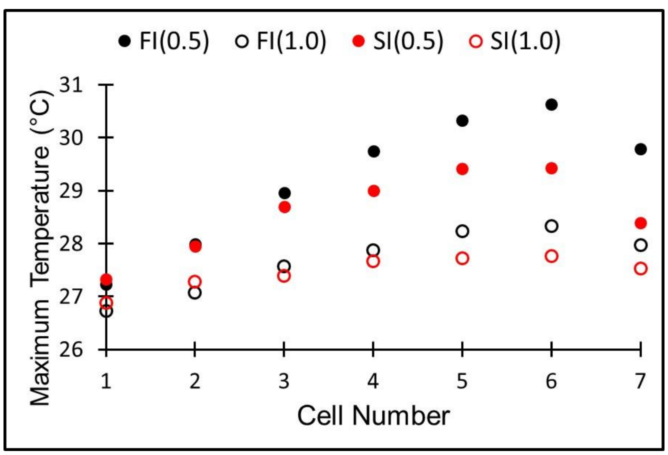

Fig. 3: Maximum temperature at individual cells. The number inside the parenthesis stands for the flow rate in LPM.

As for comparing two different TMSs in this study, overall, the SI design results in a lower cell temperature at a given flow rate. Although the cells that are closer to the inlet manifolds have almost the same maximum temperatures in both TMSs, the temperature gaps are identified at given cells (i.e., the cells at the same locations in both TMSs) that are relatively far from the inlet. For having a better insight about the cooling capability of individual TMSs, their thermal performances are compared in high and low flow rates, separately. At a higher flow rate (i.e., 1.0 LPM), the temperature gap is initially identified at Cell 5. However, due to a high sensible heat because of high flow rate, the maximum temperature gap is less than 0.6 °C. As a result, it can be concluded that both TMSs have almost the same thermal performance at high flow rates.

At the lower flow rate (i.e., 0.5 LPM), the temperature gap is initially identified at Cell 4, which is ~ 0.75 °C, and reaches to a maximum ~1.4 °C at the last cell. Larger temperature gaps in the lower flow rate are due to the lower sensible heat compared to that of the larger flow rate. In addition, the different flow patterns in two TMSs dictate the thermal performances, especially at lower flow rates. While the flow has a symmetry about the middle plane at the FI design, symmetry does not exist in the SI TMS due to the flow impingement at the inlet. Future research should address the of complex flow impingement on the thermal performance of SI TMS.

One potential benefit of the SI TMS is its high thermal performance while operating with low pumping power. The pumping power, as a key design parameter of an active cooling system, corresponds to the power required to drive the flow across the TMS [9]. Since a large pumping power may hinder using the TMS regardless of its improved thermal performance, it is crucial to minimize the pumping power. Based on Fig. 3, the SI design at 0.5 LPM leads to only ~0.4-1.2 °C hotter cells compared with the FI TMS at 1.0 LPM. Since a lower flow rate corresponds to a lower pumping power, the SI design potentially leads to a lower pumping power. Therefore, the SI design may be a more suitable TMS due to its lower pumping power but with a small penalty in heat transfer compared with the FI design. Further studies will be required to address the pressure drop in the SI TMS because the pumping power is directly proportional to the magnitude of pressure drop and flow rate.

4. Conclusion

The effects of locations of inlet and outlet manifolds on the thermal performances of two liquid-cooled TMSs were investigated. Both TMSs maintained a sufficiently low temperature variations within an individual cell as well as among all cells in a TMS. While at the higher flow rate the maximum temperature of a given cell remained almost the same in both TMSs, the SI design reduced the maximum temperature at the lower flow rate. In addition, despite a small penalty in the thermal performance of the SI design compared with the FI design, the former was identified as a promising TMS to minimize the pumping power due to its operation with half of the flow rate of the FI TMS.

Acknowledgements

The financial supports from NASA MUREP Institutional Research Opportunity (Award#80NSSC19M0196), the National Science Foundation-CREST Award (Contract #HRD-1914751), and the Department of Energy/National Nuclear Security Agency (DE-FOA-0003945) are gratefully acknowledged.

References

[1] M. Akbarzadeh, T. Kalogiannis, J. Jaguemont, L. Jin, H. Behi, D. Karimi, H. Beheshti, J. V. Mierlo, M. Berecibar, “A comparative study between air cooling and liquid cooling thermal management systems for a high-energy lithium-ion battery module,” *Appl. Therm. Eng.*, vol. 198, pp. 117503, 2021.

[2] J. Xun, R. Liu, K. Jiao, “Numerical and analytical modeling of lithium ion battery thermal behaviors with different cooling designs,” *J. Power Sources*, vol. 233, pp. 47-61, 2013.

[3] A.G. Mohammed, K. E. Elfeky, Q. Wang, “Thermal management evaluation of Li-ion battery employing multiple phase change materials integrated thin heat sinks for hybrid electric vehicles,” *J. Power Sources*, vol. 516, pp. 230680, 2021.

[4] L. H. Saw, K. Somasundaram, Y. Ye, A. A. O. Tay, “Electro-thermal analysis of Lithium Iron Phosphate battery for electric vehicles,” *J. Power Sources*, vol. 249, pp. 231-238, 2014.

[5] H. Wang, T. Tao, J. Xu, X. Mei, X. Liu, P. Gou, “Cooling capacity of a novel modular liquid-cooled battery thermal management system for cylindrical lithium ion batteries,” *Appl. Therm. Eng.*, vol. 178, pp. 115591, 2020.

[6] K. Benabdelaziz, B. Lebrouhi, A. Maftah, M. Maaroufi, “Novel external cooling solution for electric vehicle battery pack,” *Energy Rep.*, vol. 6, pp. 262-272, 2020.

[7] M.A.Bamdezh, G.R.Molaeimanesh, S.Zanganeh, “Role of foam anisotropy used in the phase-change composite material for the hybrid thermal management system of lithium-ion battery,” *J. Energy Storage*, vol. 32, pp. 101778, 2020.

[8] M. R. Shaeri, T. C. Jen, “The effects of perforation sizes on laminar heat transfer characteristics of an array of perforated fins,” *Energy Convers. Manage.*, vol. 64, pp. 328-334, 2012.

[9] M. R. Shaeri, R. Bonner, H. Pearlman, "Enhancing heat transfer rates across different flow regimes using perforated-finned heat sinks," in *Proceedings of the Second Thermal and Fluids Engineering Conference,* Las Vegas, NV, 2017, pp. 1219-1228.